

On the nuclear robustness of the r process in neutron-star mergers

Joel de Jesús Mendoza-Temis,¹ Meng-Ru Wu,¹ Karlheinz Langanke,^{2,1}
Gabriel Martínez-Pinedo,^{1,2} Andreas Bauswein,^{3,4} and Hans-Thomas Janka⁵

¹*Institut für Kernphysik (Theoriezentrum), Technische Universität Darmstadt,
Schlossgartenstraße 2, 64289 Darmstadt, Germany*

²*GSI Helmholtzzentrum für Schwerionenforschung, Planckstraße 1, 64291 Darmstadt, Germany*

³*Department of Physics, Aristotle University of Thessaloniki, 54124 Thessaloniki, Greece*

⁴*Heidelberger Institut für Theoretische Studien, Schloss-Wolfsbrunnengasse 35, 69118 Heidelberg, Germany*

⁵*Max-Planck-Institut für Astrophysik, Postfach 1317, 85741 Garching, Germany*

We have performed r-process calculations for matter ejected dynamically in neutron star mergers based on a complete set of trajectories from a three-dimensional relativistic smoothed particle hydrodynamic simulation with a total ejected mass of $\sim 1.7 \times 10^{-3} M_{\odot}$. Our calculations consider an extended nuclear network, including spontaneous, β - and neutron-induced fission and adopting fission yield distributions from the ABLA code. In particular we have studied the sensitivity of the r-process abundances to nuclear masses by using different models. Most of the trajectories, corresponding to 90% of the ejected mass, follow a relatively slow expansion allowing for all neutrons to be captured. The resulting abundances are very similar to each other and reproduce the general features of the observed r-process abundance (the second and third peaks, the rare-earth peak and the lead peak) for all mass models as they are mainly determined by the fission yields. We find distinct differences in the predictions of the mass models at and just above the third peak, which can be traced back to different predictions of neutron separation energies for r-process nuclei around neutron number $N = 130$. In all simulations, we find that the second peak around $A \sim 130$ is produced by the fission yields of the material that piles up in nuclei with $A \gtrsim 250$ due to the substantially longer beta-decay half-lives found in this region. The third peak around $A \sim 195$ is generated in a competition between neutron captures and β decays during r-process freeze-out. The remaining trajectories, which contribute 10% by mass to the total integrated abundances, follow such a fast expansion that the r process does not use all the neutrons. This also leads to a larger variation of abundances among trajectories as fission does not dominate the r-process dynamics. The resulting abundances are in between those associated to the r and s processes. The total integrated abundances are dominated by contributions from the slow abundances and hence reproduce the general features of the observed r-process abundances. We find that at timescales of weeks relevant for kilonova light curve calculations, the abundance of actinides is larger than the one of lanthanides. This means that actinides can be even more important than lanthanides to determine the photon opacities under kilonova conditions. Moreover, we confirm that the amount of unused neutrons may be large enough to give rise to another observational signature powered by their decay.

PACS numbers: 26.30.Hj, 26.50.+x, 97.60.Jd

I. INTRODUCTION

The astrophysical r process produces about half of the heavy elements in the Universe, including all of the actinides [1, 2]. It is commonly accepted that it occurs as a sequence of neutron captures and β decays in environments with extreme neutron densities. Under such conditions neutron captures are much faster than β decays and the r-process path runs through nuclei with large neutron excess far off stability [3, 4].

The actual astrophysical site of the r process is yet not known. For many years the neutrino-driven wind from the surface of a freshly born neutron star in a core-collapse supernova has been the favored site [5]. However, recent supernova simulations with improved nuclear input, realistic neutrino transport and advanced multi-dimensional treatment of hydrodynamics [6] indicate that the conditions of the matter ejected in the wind (entropy, expansion velocity, proton-to-neutron ratio) are not suited to support an r process which produces the el-

ements in the third peak (around mass number $A \sim 195$) and beyond. However, the neutrino-driven wind might significantly contribute to the abundance of the lighter elements up to the second peak ($A \sim 130$) [7–9]. The shortfall of the neutrino-driven wind model to produce the heavier r-process elements has revived the interest in another potential site, the merger of two neutron stars (NS merger) [10, 11].

Simulations of NS mergers indicate that the matter ejected during the dynamical phase is very neutron rich with extremely large neutron-to-seed ratios ($R_{n/s} > 400$) [12–14]; i.e. there are many neutrons which can be captured by seed nuclei transporting matter to very heavy nuclei in the region of the nuclear chart where decay by fission is possible. The intermediate-mass fission yields are then subject to neutron captures establishing the occurrence of a few fission cycles, which are expected to produce the heavier r-process elements in a rather robust way with nearly relative solar abundances. We note that such a robust scenario is quite attractive as it might

explain the occurrence of r-process elements above the second peak in solar proportion as observed in very old metal-poor stars [15]. Recent simulations suggest that the electron fraction of part of the ejecta may be raised by neutrino processes [16–18]. However, the sensitivity of these results to the treatment of neutrino radiation transport in NS mergers simulations remains to be explored. In this study, we work under the assumption that all ejecta remain neutron rich.

An additional source of ejected material with relevance for r-process nucleosynthesis comes from the accretion disk formed around the compact object resulting from the merger. However, the conditions in these ejecta are more sensitive to the details of the astrophysical parameters and microphysics included [19–22]. Here we will consider only the initial dynamical ejecta.

To serve as the site for the production of heavy r-process elements and to explain the observation of the elemental abundances in solar proportion in metal-poor stars, the r process in NS mergers should not depend on particular astrophysical conditions, e.g. on the specific combination of NS masses in the merging binary system. It is unsatisfactory for r-process abundance simulations that most nuclei encountered during the process have yet not been produced in the laboratory and hence their properties depend on nuclear models and are yet quite uncertain.

The sensitivity of r-process nucleosynthesis in dynamical ejecta of NS mergers to the astrophysical conditions, i.e. neutron star masses, orbit parameters, has been studied in [12–14, 17]. Korobkin *et al.* have performed r-process simulations for a set of NS mergers consisting of various combinations of neutron stars in the relevant mass range between 1 and 2 M_{\odot} [13], while Bauswein *et al.* have explored the influence of various equations of state on the merger dynamics and nucleosynthesis [14] (see also ref. [17]). It turns out that the specific treatment of the merger dynamics, e.g. Newtonian vs General Relativistic mechanics, leads to fundamentally different mass ejection dynamics [13, 14]. Importantly for our discussion both groups find, within their treatment, nearly identical abundance distributions between the second and third peaks for all of the 23 combinations of neutron stars [13] or the various adopted equations of state [14], pointing to virtually no sensitivity of the relative abundance of heavy elements on the astrophysical conditions of the mergers. However, both groups also found strong sensitivity of the abundances to the treatment of fission. Indeed, the calculations of [13] show an abundance hole around $A \sim 140$, relative to solar, while in the study of ref. [14] the second peak is noticeably shifted to larger mass numbers. Both effects are related to the treatment of fission adopted in the respective simulations.

This dependence on fission as well as the effect of half lives and neutron separation energies (masses) on the r-process abundances in NS merger simulations has been the focus of three simultaneous and independent studies. Eichler *et al.* have confirmed the strong sensitiv-

ity on the fission yield distribution [23]. However, they succeeded to show that fission yields derived with the ablation-abrasion model code ABLA [24, 25], which is based on the statistical model, cured the shortcomings in the abundance distribution above the second peak. The ABLA code is adjusted to reproduce fission data and considers the evaporation of free neutrons before and after the fission process. However, these neutrons as well as those which are produced by the decay of the fission fragments can be captured by nuclei after freeze-out resulting in a slight shift of the third peak to heavier mass numbers than is observed in the solar abundances. Eichler *et al.* [23] argue that such a shift can be avoided by faster β decays than those predicted by the Finite Range Droplet Model (FRDM) model which has been adopted in their study. In an independent study Caballero *et al.* come to the same conclusion [26] when they compare results of NS merger r-process simulations performed with the half lives based on the FRDM model with those obtained by replacing these half lives with faster values derived by QRPA calculations on top of the energy density functional (EDF) of Fayans [27]. Importantly, these faster EDF-based half lives agree well with recent experimental data obtained for nuclei close and on the r-process path, including data for neutron-rich nuclei towards the $N = 126$ waiting points [28]. Here, the EDF-based half-lives, in close agreement with recent large-scale shell model calculations [29, 30], point to the importance of forbidden transitions to the β decays.

In this manuscript, we study the effect of nuclear masses and neutron capture rates on the r process in NS mergers. Masses are particularly important as they, via the neutron separation energies, define the r-process path in the nuclear chart and secondly they are crucial ingredients in the statistical model calculation of neutron capture cross sections. In the following we will derive neutron separation energies as well as neutron capture cross sections consistently from the same mass models. Furthermore photodissociation cross sections are obtained by detailed balance from the capture cross sections. As the masses of the extremely neutron-rich nuclei on the r-process path are not known experimentally, they have to be modeled. For many years, masses derived on the basis of the Finite Range Droplet Model (FRDM) [31] and the ETFSI model (Extended Thomas Fermi Model with Strutinski Integral [32]) have been a standard in r-process simulations. Recently Wang and Liu developed an alternative microscopic-macroscopic mass model (Weizsäcker-Skyrme or WS3 model [33]), which employs a Skyrme energy density formula as a macroscopic basis, which is then microscopically supplemented by shell corrections. Guided by intuition derived from the interacting shell model, Duflo and Zuker developed a mass formula based on a systematic description of occupation numbers and taking special care of the role of intruder states [34]. In this work we will use the Duflo-Zuker mass formula with 31 parameters (DZ31). Finally advances in computing resources make it now possible to derive mass formulas

on the basis of microscopic nuclear many-body models, like the Hartree-Fock-Bogoliubov (HFB) model. In a sequence of continuous improvements of the Skyrme functional, which is the basis of their model, Goriely and collaborators have succeeded to obtain an HFB mass model which is comparative to the phenomenological models, like FRDM and ETFSI, and can be globally applied in r-process simulations [35]. In our calculations, we will use the model HFB21 [36].

The sensitivity of the r-process abundances in NS mergers to variations of nuclear masses has, so far, been insufficiently explored. There are calculations in the literature based on different mass models but it is often difficult to compare the results due to a combination of factors including rather different assumptions about the astrophysical conditions, different approaches for the calculation of the relevant neutron capture rates, and/or the use of very different fission yield distributions. In this work, we aim at exploring how robust the r-process abundances are against variations of the nuclear masses keeping the astrophysical conditions unchanged. We use four different mass models (FRDM, WS3, DZ31, HFB21) for the calculation of the neutron capture rates that enter in the r-process simulations. Furthermore, we aim at determining the nuclear origin of the robust r-process pattern observed in several neutron star merger simulations. It is often stated that NS mergers produce a robust r process due to fission cycling. However, this statement simply expresses the fact that fission cycling is unavoidable due to the large neutron-to-seed ratios reached in NS merger ejecta without really explaining the nuclear mechanism responsible for the robustness.

We have used the full set of trajectories based on a 3-dimensional relativistic simulation of the merger of two neutron stars with $1.35 M_{\odot}$, which is expected to be the most frequent NS merger system. Although these trajectories cover a broad range of dynamical parameters, including a large variation in neutron-to-seed values, we will argue that they can be best classified into two categories with respect to their final nucleosynthesis abundance yields: i) For the majority of trajectories neutrons are nearly completely depleted at the end of r-process nucleosynthesis, producing significant abundances of heavy nuclei in the fissioning region, which, in turn, produce the $A \sim 130$ peak in the r-process abundance distribution by their decay yields. The resulting r-process abundances show quite similar patterns. ii) Around 10%, in mass, of the trajectories follow a very fast expansion. The associated low matter densities result in the fact that not all neutrons have been captured at the end of the r process [20, 37]. In this scenario the abundance of heavy nuclei in the fissioning region is rather low and the second r-process peak ($A \sim 130$) is a consequence of stalled matter flow due to the relatively long half-lives of nuclei in the vicinity of the magic neutron number $N = 82$. In this scenario the final r-process abundance distribution is rather sensitive to nuclear structure effects.

We stress that our results should not be considered

as a prediction of the typical r-process yields from NS mergers to be used in chemical evolution studies. This will require a complete set of trajectories for both the dynamical and disk ejecta as done in ref. [20].

Our paper is organized as follows. In the next section we give a brief description of our r-process simulations and the input being used. The results of our simulations for the r-process abundances and their dependence on the adopted mass models are presented and discussed in section III. Finally, we conclude in section IV.

II. NS MERGER TRAJECTORIES AND NUCLEAR INPUT

The r-process calculations in this work are based on fluid element trajectories that were extracted from hydrodynamical simulations of NS mergers to represent the conditions of matter becoming unbound from such events. The merger simulations were performed with a three-dimensional relativistic smoothed particle hydrodynamics code [14, 38–40], which imposes conformal flatness on the spatial three-metric to solve the Einstein equations in an approximate manner [41, 42]. The calculations started from initial data representing close binary systems in quasi-equilibrium a few orbits before merging. Initially the NS matter was in neutrino-less beta-equilibrium at zero temperature. The initial electron fraction was advected with the fluid during the hydrodynamical simulations without taking into account neutrino processes. This simplification was a reasonably good approximation in Newtonian models (e.g. [43]), but the impact of neutrinos in relativistic merger models requires further investigation [16–18]. NS matter is modelled with the TM1 EoS [44–46], which leads to a NS radius of 14.49 km for a $1.35 M_{\odot}$ NS and a maximum gravitational mass of $2.21 M_{\odot}$ for non-rotating NSs.

In this work we focused on a binary system of two NSs with gravitational masses of $1.35 M_{\odot}$, which may be representative for the observed double NS systems (see e.g. [47] for a compilation of measured binary NS masses). In the simulation we found most unbound matter originating from the contact interface during the coalescence (see [14] for a detailed description of the merger dynamics and ejection mechanism). Originating from the inner NS crust these ejecta are very neutron-rich. The time-step limitations of the NS simulations allowed to follow the ejecta only up to $t = t_0 \sim$ several 10 milliseconds. Hence, we have analytically continued the trajectories for $t > t_0$ by evolving the density assuming a homologous expansion, i.e. $\rho(t) = \rho(t_0) (t_0/t)^3$.

We have calculated the r-process abundances for 528 trajectories with a total mass of $\sim 1.70 \times 10^{-3} M_{\odot}$. As we will show below, the r-process nucleosynthesis dynamics and its final abundance distribution implies to classify the trajectories with respect to two competing rates: the depletion rate due to neutron captures on seed nuclei and the hydrodynamic expansion rate. The neutron depletion

rate λ_n can be approximated by

$$\lambda_n = \frac{d(\ln Y_n)}{dt} \approx \frac{\rho Y_s}{m_u} \langle \sigma v \rangle = \frac{\rho Y_n}{m_u R_{n/s}} \langle \sigma v \rangle, \quad (1)$$

where $Y_{n(s)}$ is the number fraction of neutrons (seed nuclei) and $\langle \sigma v \rangle$ is the neutron capture rate averaged over the seed nuclei. The hydrodynamic expansion rate for homologous expansion can be calculated by

$$\lambda_d = -\frac{d(\ln \rho)}{dt} = \frac{3}{t}. \quad (2)$$

For most of the ejecta (484 trajectories with a total mass of $\sim 1.57 \times 10^{-3} M_\odot$), nearly all initial neutrons can be captured as $\lambda_n \gtrsim \lambda_d$ until the end of the r process at ~ 1 s. This implies that the density should be larger than a threshold value to allow for the complete capture of neutrons: $\rho_{\text{th}} \approx 0.5 \text{ g cm}^{-3}$ at $t \sim 1$ s for typical values of $Y_n \sim 1$, $\langle \sigma v \rangle \sim 10^{-20} \text{ cm}^3 \text{ s}^{-1}$, and $R_{n/s} \sim 10^3$. We will call these trajectories “slow ejecta” in the following. They are labelled by grey curves in Fig. 1. On the other hand, about $\sim 10\%$ of the ejecta (44 trajectories, $\sim 1.28 \times 10^{-4} M_\odot$) initially expand extremely fast for a few ms reaching density values lower than the threshold discussed above. This results in a neutron depletion rate smaller than the hydrodynamic expansion rate. As a consequence free neutrons are left at the end of the r process, which may potentially influence the observed light curves of the ejecta due to the decay of neutrons [37]. In the following we will call these trajectories “fast ejecta”. They are labelled by brown curves in Fig. 1.

We have started our r-process calculations at temperatures of $T = 6$ GK, with densities ranging from $\rho \sim 10^7 \text{ g cm}^{-3}$ to $\sim 3 \times 10^{13} \text{ g cm}^{-3}$. The initial matter compositions have been determined assuming the matter to be in Nuclear Statistical Equilibrium (NSE). The initial neutron-to-seed ratios ($R_{n/s}$) of those ejecta range from 400 to 2000.

While the details of the initial composition depend on the conditions of the trajectories and on the mass models used, we can generally observe that they are given by neutron-rich nuclei centered around magic neutron numbers $N = 50$ and $N = 82$, while proton numbers in the iron-nickel range are favored in the first case and around strontium-zirconium in the second. The relative weight of these two composition peaks depends on entropy, favoring the peak around mass number $A \sim 120$ relative to the one around $A \sim 80$ with decreasing entropy.

Starting from these initial compositions we have followed the r-process evolution by a large network. The dynamics of the process was governed by the astrophysical trajectories, however, consistently corrected for reheating by energy release in nuclear reactions, as we describe below. Our network includes more than 7300 nuclei which cover the nuclear chart from free nucleons up to ^{313}Ds . As nuclear reactions among these nuclei we considered charge particle reactions, neutron captures and its inverse process, photo-dissociation, and β and α decay and fission. We have derived the neutron capture

rates consistently for each individual mass model within the statistical model using the code MOD-Smoker [48]. The photodissociation rates were obtained from the neutron capture rates by detailed balance. For nuclei, for which the half lives are not known experimentally, we have adopted the β decay (and β delayed neutron emission) rates from the compilation of Möller *et al.* [49], which was derived from QRPA calculations on top of the FRDM mass model. We used the parametrization of Ref. [50] of the Viola-Seaborg formula to estimate the α -decay rates, which become relevant for heavy nuclei beyond lead. Finally, for nuclei with $Z > 83$, where a competition between (n, γ) and neutron induced fission can take place, we used neutron-induced reaction rates taken from [51] that are based on the FRDM mass model [31] and the Thomas-Fermi fission barriers of Myers and Swiatecki [52]. Rates for β delayed and spontaneous fission were adopted from [53]. Our fission yields were taken from the calculations of Ref. [54] which were derived using the code ABLA. This approach also gives a consistent estimate for the number of neutrons set free during the fission process.

Nuclear reactions change the energy balance of the environment. We take this into account following refs. [11] by calculating, at any time of the evolution, the change in abundances in the various nuclei by solving the nuclear network. The related energy release is mainly connected to β decays where we assume that half of the energy set free in the process is carried away by the neutrino [55, 56]. In the next step, the energy release can be translated into a change of entropy, from which we calculated a new temperature using the equation of state of Ref. [57] which considers nucleons, nuclei, electrons, positrons and photons.

III. RESULTS

A. Time evolution and energy generation

We have started our r-process simulations for all trajectories at temperatures $T = 6$ GK assuming an initial NSE composition. As a striking feature, we note the very large neutron-to-seed ratios ($R_{n/s} \approx 400 - 2000$) which is a prerequisite of r-process nucleosynthesis for nuclides beyond the third peak reaching the region in the nuclear chart where nuclei decay by fission. Furthermore, due to the extremely high neutron densities involved, the path of the r process in NS mergers runs through nuclei close to the dripline. For these nuclei, with their large Q values, β decays are fast (order ms or faster).

Before we study the nucleosynthesis results of our simulations we like to make some important remarks concerning the heating of the astrophysical medium by nuclear reactions, mainly by β decays. In Fig. 1 we show the evolution of density, temperature and the energy release due to nuclear reactions for all trajectories and the different mass models considered.

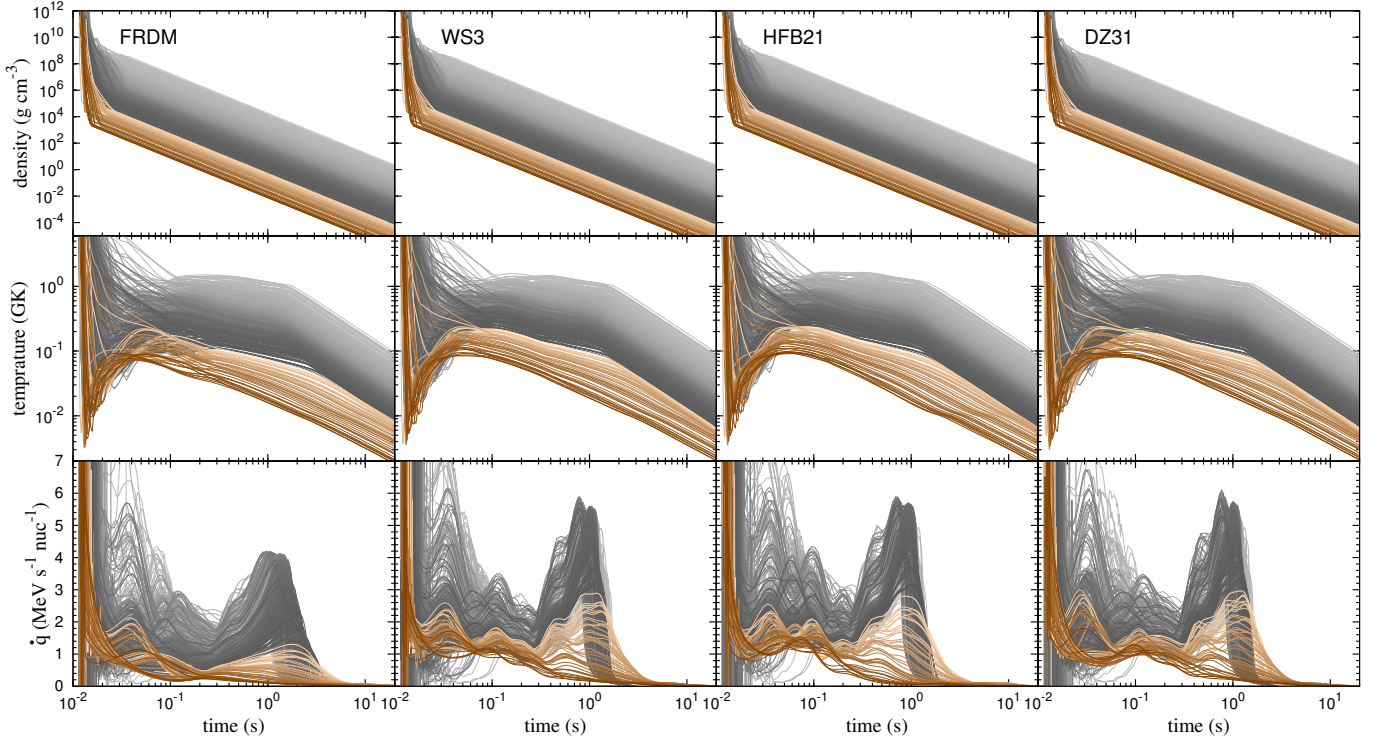


FIG. 1. (Color online) Evolution of the different thermodynamical variables for all trajectories for different mass models. The gray (brown) curves correspond to the “slow (fast) ejecta” (see text for the definition). The upper panels show the evolution of density that is identical for all cases. The middle panel shows the evolution of temperature that considers the feedback due to the energy generation shown in the lower panel.

The density and temperature profiles of the trajectories are shown in Fig. 1. The temperature evolution of the trajectories shows some characteristic pattern which we will discuss in the following. For most of the trajectories, the temperature initially drops to a minimum in the first few tens of ms and later rises to a maximum during the r process. This behavior can be understood from basic thermodynamics. From the first law of thermodynamics the energy per nucleon released by nuclear reactions, \dot{q} , is related to the change of the energy per nucleon, ε and nucleon density, $n = \rho/m_u$ (m_u the atomic mass unit), as:

$$\dot{q} = \frac{d\varepsilon}{dt} - \frac{P}{n^2} \frac{dn}{dt} = c_V \frac{dT}{dt} + \left(\frac{d\varepsilon}{dn} - \frac{P}{n^2} \right) \frac{dn}{dt}. \quad (3)$$

where $c_V = d\varepsilon/dT$ is the specific heat per nucleon at constant volume. The evolution of temperature reduces to:

$$\frac{dT}{dt} = \frac{1}{c_V} \left[\dot{q} - \frac{1}{\tau_n} \left(\frac{P}{n} - n \frac{d\varepsilon}{dn} \right) \right] \quad (4)$$

where we have introduced the expansion timescale $\tau_n = 1/\lambda_d$. At early times when material expands from high densities, the expansion time scale is rather small $\tau_n \approx 1$ ms and the second term in the bracket dominates

and consequently the temperature decreases as the material expands. However, as the expansion proceeds and the temperature decreases there will be a moment at which both terms on the right hand side become of the same magnitude. This will correspond to a minimum in the temperature that can be estimated assuming an equation of state dominated by nuclei (Boltzmann ideal gas) and radiation (photons). In this case, we have

$$\varepsilon = \frac{3}{2} \frac{kT}{A} + \frac{aT^4}{n} \quad (5a)$$

$$P = \frac{nkT}{A} + \frac{1}{3} aT^4 \quad (5b)$$

At initial times the average mass number A is about 1, and it grows as the r process proceeds. Substituting in equation (4) we have:

$$\frac{dT}{dt} = \frac{1}{c_V} \left[\dot{q} - \frac{1}{\tau_n} \left(\frac{4aT^4}{3n} + \frac{kT}{A} \right) \right] \quad (6)$$

The minimum of temperature is reached when the right hand side of the above equation is zero. Initially, when the density is relatively high, the second term in the inner parentheses dominates and we have:

$$T_{\min} = 0.05 \text{ GK} \left(\frac{\dot{q}}{4 \text{ MeV s}^{-1}} \right) \left(\frac{\tau_n}{1 \text{ ms}} \right) \left(\frac{A}{1} \right) \quad (7)$$

for the minimal temperature assuming typical values for the other quantities. We see that the minimum temperature is proportional to the expansion timescale. This fact can be understood by noticing that during the expansion the energy generation can only contribute efficiently to increase the temperature during a period of time τ_n . Once the minimum value is reached the temperature starts to rise favored by the fact that the timescale for the expansion grows. However, as the temperature increases and the density decreases the first term in the inner brackets of equation (6) increases. A maximum in temperature is reached once the equation of state becomes dominated by radiation corresponding to a temperature of

$$T_{\max} = \left(\frac{3n\dot{q}\tau_n}{4a} \right)^{1/4} \quad (8)$$

$$= 0.8 \text{ GK} \left[\left(\frac{\rho}{10^5 \text{ g cm}^{-3}} \right) \left(\frac{\dot{q}}{4 \text{ MeV s}^{-1}} \right) \left(\frac{\tau_n}{10 \text{ ms}} \right) \right]^{1/4},$$

where we have used typical values for the density, energy generation and expansion timescale. The above discussion clearly shows that the behavior of temperature is determined by basic thermodynamics and it is driven by the fact that at high densities the EoS is dominated by the ideal gas component while at low densities radiation dominates. The dominance of radiation implies a rather large specific heat $c_V \approx 4aT^3/n$ that reduces the efficiency at which the energy generation can contribute to temperature increase. This means that the maxima in temperature is rather flat as observed in the simulations and depends on the expansion timescale at times $0.1 \text{ s} \lesssim t \lesssim 1 \text{ s}$.

For some trajectories matter is being heated by the shock to temperatures $T \gtrsim 6 \text{ GK}$ at rather low densities $\rho \sim 10^8 \text{ g cm}^{-3}$. For these cases, radiation quickly dominates the contribution to the total energy such that the temperature directly approaches T_{\max} (as a saddle point) without exhibiting a minimum.

We like to stress that, for a given trajectory and independent of the early phase of the temperature evolution, the temperature during the r process is rather determined by the density and the expansion time-scale, as can be seen from Eq. (8). We have confirmed this in our calculations by varying the initial temperature for the r-process simulations between 3 GK and 10 GK. We find that the early temperature evolution depends on the initial conditions. However, in the later evolution, which is crucial for r-process nucleosynthesis, the temperature profiles converge to rather similar conditions caused by the balance of nuclear heating and radiation dominance. One can say that the material loses the memory of the particular thermodynamical conditions when it was ejected. This aspect together with the large neutron-to-seed ratio, which makes the nucleosynthesis insensitive to the initial composition, is fundamental to achieve a robust r-process pattern in dynamical ejecta

After the r-process comes to an end with matter decaying back to stability (this occurs after $\sim 1\text{-}2 \text{ s}$ for the slow ejecta and $\lesssim 10 \text{ s}$ for the fast ejecta), the energy release due to nuclear reactions drops and the temperature follows an adiabatic expansion that for the radiation dominated conditions implies $T \sim \rho^{1/3}$. It is important to note that the temperature of nearly 10^9 K , which may be achieved during most of the r process due to nuclear reheating, is sufficient to establish an $(n, \gamma) \rightleftharpoons (\gamma, n)$ equilibrium for a significant part of the trajectories, shown in Figure 1.

The energy release shows quite distinct peak structures as function of time. These differences are substantial as a function of mass model. However, they lead to only minor differences in the evolution of temperature as discussed above. The peaks are related to matter being accumulated and then breaking through the r-process waiting points at the magic neutron numbers, where fission cycling, which we will quantify below, induces repetitions of these processes.

B. Evolution of the r-process abundances for the slow ejecta

We have studied r-process nucleosynthesis for the set of 528 NS merger trajectories and for 4 different mass models. The calculated r-process abundances show quite similar general patterns for all mass models. In this subsection, we discuss the special features of r-process nucleosynthesis of the so-called slow ejecta. The next subsection then deals with r-process nucleosynthesis for the fast-evolving ejecta. For the slow ejecta we show the abundances at 3 different phases of the evolution: a) at freeze out, which we define as the moment where $R_{n/s} = 1$, b) the moment when the average timescale for β decays becomes equal to the average timescale for neutron captures, c) the final abundance, calculated at a time of 1 Gyr.

Comparing the abundances at these 3 different phases for the slow ejecta (shown in Fig. 2) we observe the following important features. At freeze-out, the abundances show a strong odd-even staggering which is washed out subsequently by continuing neutron captures and β decays towards stability. The magnitude of the staggering is much larger for those trajectories that achieve an $(n, \gamma) \rightleftharpoons (\gamma, n)$ equilibrium, light gray lines, compared with those which follow cold r-process conditions, dark gray lines. Strikingly, there is no abundance peak at $A \sim 130$, in contrast to the third peak at $A \sim 195$ (the narrow peak at around 136 is seen only in FRDM and will be discussed below). The matter flow through the second peak is faster than through the third peak. The origin of this difference is that even at the same neutron separation energy, Q_β values are larger at the $N = 82$ nuclei on the r-process path than for the $N = 126$ nuclei making the respective half-lives significantly shorter. The second abundance peak is produced mainly by fission yields from

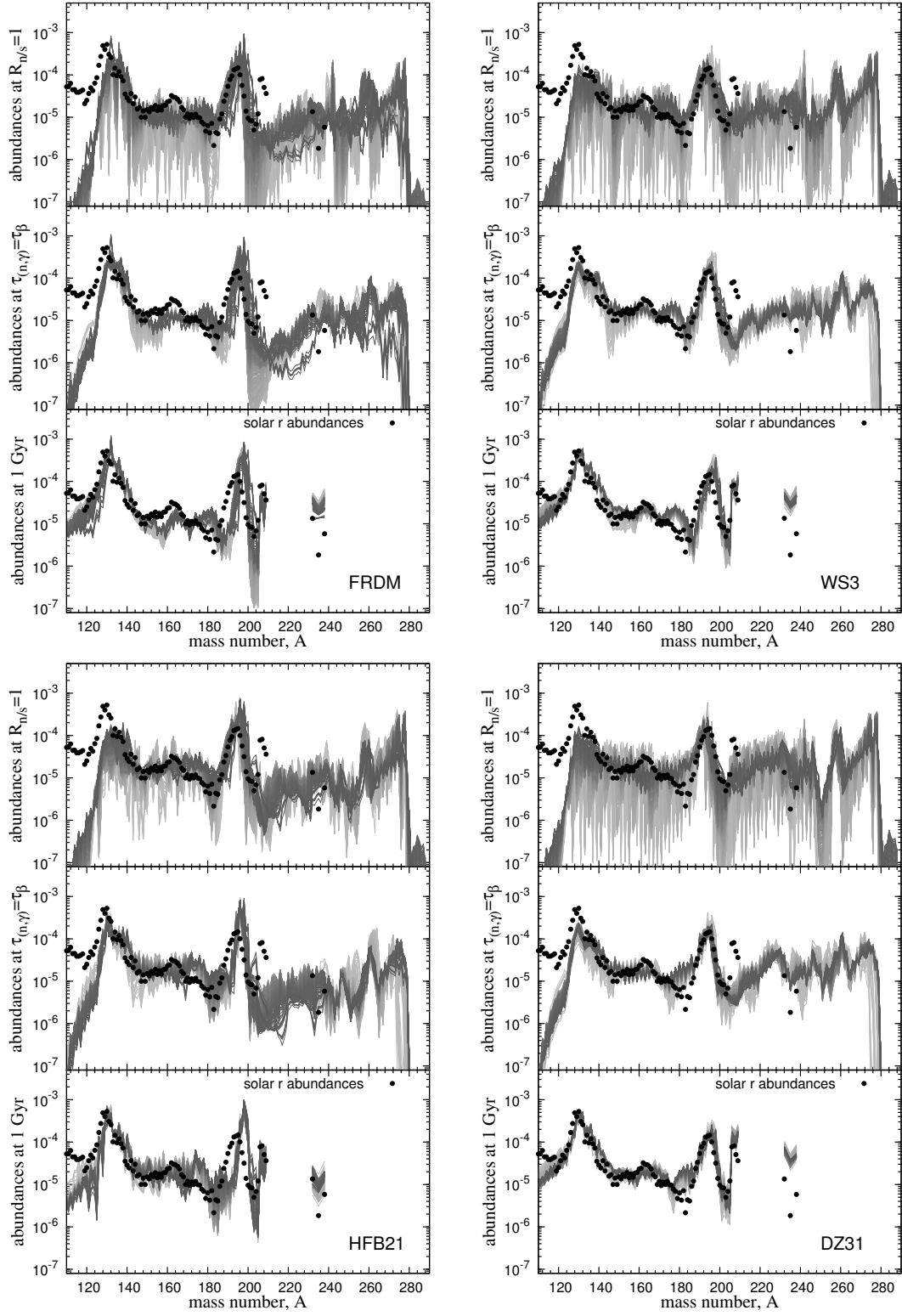


FIG. 2. (Color online) R-process abundances of the slow ejecta for different mass models at different phases of the evolution. The upper panels show the abundances at $R_{n/s} = 1$. The middle panel at the time where the average timescales for beta-decay and neutron captures become identical. The lower panel shows the abundances at 1 Gyr when most of the material has already decayed to the stability.

heavy nuclei around $A \sim 280$ associated with the magic neutron number $N = 184$. At freeze-out, however, there is still a sufficient reservoir of free neutrons from fission and subsequent β decay and photodissociation to support further neutron captures, also on nuclei around $A \sim 130$. These neutron captures (note that $\tau_\beta > \tau_{(n,\gamma)}$ at freeze out) shape the abundances after freeze out significantly as can be seen when comparing the upper and middle panels in Fig. 2. Importantly, we observe that the second peak now forms (as transport from the fission yields to heavier nuclei by neutron captures is reduced). Furthermore, the strong abundance hole just above $A \sim 195$ is filling up due to decays of heavier nuclei (mainly α decays of nuclei between lead and thorium). At the time of 1 Gyr, final abundances for mass numbers $A > 120$ are virtually identical, for a given mass model, for all slow ejecta as shown in the bottom panels. This points to an extremely robust mechanism in shaping the final abundance pattern nearly independent of the initial large variation of the astrophysical condition which will be further discussed in III D. Below in this subsection, we will focus on the detailed discussion of the nuclear physics properties that give rise to the variation seen in different nuclear mass models.

At freeze-out the nuclei with largest abundances in the transuranium region are located around $A \sim 280$ corresponding to the $N = 184$ shell closure. The lightest nuclei for which neutron separation energies are large enough to allow matter flow beyond $N = 184$ is ^{279}Am . However, for this nucleus the fission barrier is so low that neutron-induced fission on ^{278}Am dominates over neutron capture and the r-process cycles to medium mass nuclei rather than producing heavier nuclei. Correspondingly, the nucleus with maximum mass produced in our calculations is ^{278}Pu that decays by beta-emission subsequently followed by neutron-induced fission on ^{278}Am . The corresponding fragment distributions as a function of mass, charge and neutron number are shown in figure 3, indicating that one of the fragments contributes to the second peak r-process abundances while the other is produced around $A \sim 140$. Subsequent neutron captures and beta-decays distribute the contribution of this second fragment to higher masses.

Fission is also an important source of free neutrons. The total number of neutrons produced can be divided into two components. A prompt component that consists of the neutrons evaporated mainly by the highly excited fragments. For neutron-induced fission on ^{278}Am , ABLA predicts a prompt emission of 7 neutrons. In addition to the prompt neutron emission, there is a delayed component that occurs during the decay of the fragments to the instantaneous r-process path. This delayed component depends on the location of the fragments relative to the r-process path and the dominating reaction mechanism (beta-decay or photodissociation). Both the r-process path and the reaction mechanism sensitively depend on the astrophysical conditions, particularly on the temperature. If the temperature is

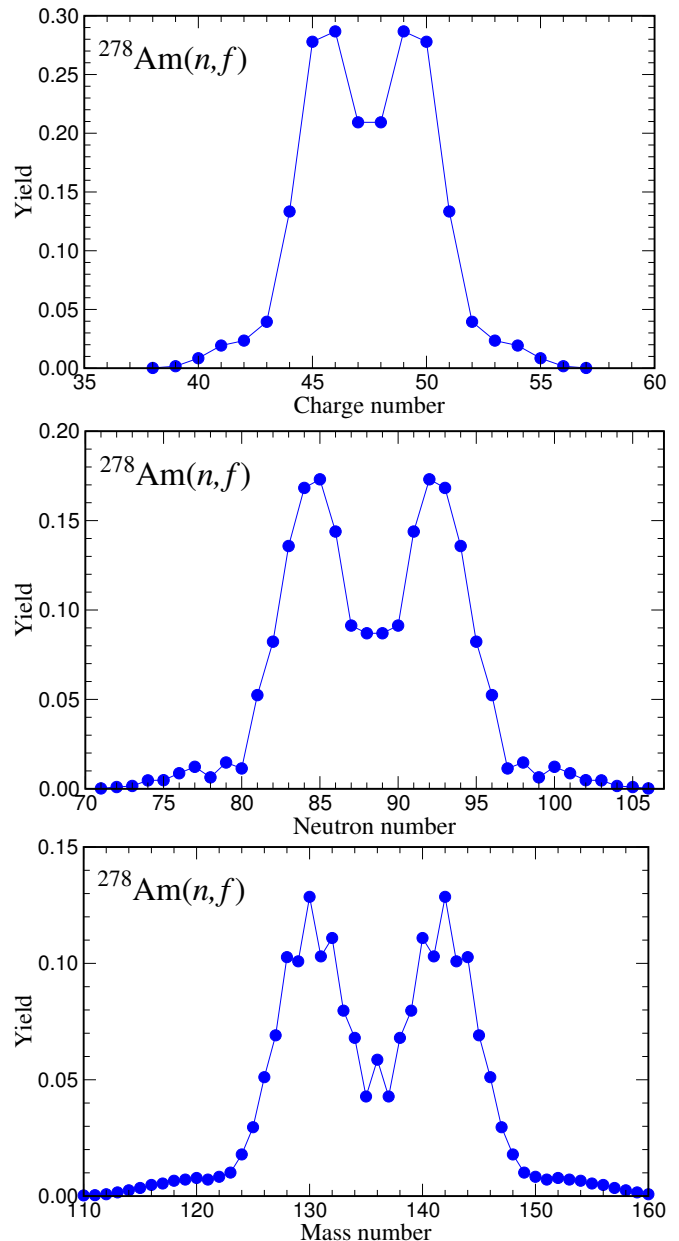


FIG. 3. (Color online) Fission fragment distributions as functions of charge, neutron number, and mass number for neutron induced fission on ^{278}Am as predicted by the ABLA code.

large enough, photodissociation is the dominating reaction mechanism. Under these conditions the number of free neutrons produced is fully determined knowing the charges Z_1 and Z_2 of the produced fragments and is given by $n_{\text{prod}} = A_f - A_{\text{path}}(Z_1) - A_{\text{path}}(Z_2)$, where A_f is the mass number of the fissioning nucleus and $A_{\text{path}}(Z)$ is the mass number of the nucleus with charge Z on the instantaneous r-process path. This means that for the assumed astrophysical conditions, the total number of free neutrons is completely determined by the charge fragment distribution of the fission process. While photodissociation is the dominating reaction mechanism at suffi-

ciently high temperatures, beta-delayed neutron emission becomes increasingly important with decreasing temperature. In this case, the total number of neutrons produced will depend on the prompt component predicted by the fission model and the chain of beta-decays occurring during the decay to the instantaneous r-process path.

Once neutron captures are slower than β decays, matter decays to stability. In particular, the significant amount of matter above lead, still existing in the middle panels of figure 2, decays to finally form the lead peak. At 1 Gyr only the long-lived thorium and uranium isotopes survive. When comparing the time evolution of the third peak (from the upper to the middle to the lower panel of figure 2) one clearly notices a shift of the third peak to slightly larger mass numbers in the FRDM mass model. This is caused by neutron captures after freeze-out and confirms the findings reported in [23]. Looking at the final abundances computed for the mass models used in the present study (see Fig. 6) we observe that the shift in the third r-process peak is present in the FRDM and HFB21 mass model but absent in the WS3 and DZ31 mass models. To understand the reason for this behavior it is important to qualitatively quantify which regions of the nuclear chart are expected to be more relevant for the evolution of the r process under very general assumptions.

The r process operates along a path of almost constant neutron separation energy. The speed at which the r process proceeds from lighter nuclei to heavier nuclei depends on the beta-decay half-lives. Due to the increase in Coulomb energy the valley of stability moves to more neutron rich nuclei with increasing charge number. This means that for a line of constant neutron separation energy the beta-decay Q-values reduce with increasing charge. As a consequence, the beta-decay half-lives of r-process nuclei increase with increasing mass number. On top of this global behavior, there are local effects induced by the presence of neutron shell closures. In particular, at neutron magic numbers $N = 82$ and $N = 126$ the r process moves closer to stability to nuclei with longer beta-decay half-lives. In the r-process path nuclei with $N \gtrsim 82$ and $N \gtrsim 126$ have the longest half-lives. At freeze-out, it corresponds to charge numbers $Z \approx 48$ and $Z \approx 70$, respectively. The predicted half-lives of these nuclei [29] are of the order of 100 ms which is not much less than the total duration of the r process, namely around 1 s. Changing the time the r process expends in this long-lived nuclei affects the whole dynamics of the r process and consequently impacts the r-process abundances. This timescale can be affected by modifications of individual beta-decay half-lives that so far are based on relatively uncertain theoretical approaches [49, 58]. Alternatively, the effective r-process timescale in the region can change if the r-process path changes due to modifications of the underlying mass model. This is the aspect explored in this work.

Different mass models differ substantially in their pre-

dictions in regions where there is a sudden change in the intrinsic deformation [59]. This is particularly the case around $N \sim 90$ and $N \sim 130$ where all mass models used in the present work predict a transition from spherical to deformed configurations. The particular relevance for the r process is the fact that this transition can be associated with a sudden drop in the neutron separation energies. This is the case for the FRDM mass model as was already pointed out in Ref. [60] for the Tellurium isotopes reaching ^{139}Te . Recent mass measurements for Tellurium isotopes [61, 62] have ruled out this sudden drop in neutron separation energies. However, at present there is no data for lighter isotopes in the region where FRDM also predicts very low neutron separation energies [59]. None of the other models used in the present study show such a drastic reduction in neutron separation energies around $N = 90$. The most noticeable consequence is the presence of a narrow peak around $A \sim 136$ at freeze-out (see upper panel for FRDM mass model in Fig. 2). Due to the accumulation of material in this region, the r process lasts slightly longer using the FRDM mass model when compared with the other models (see Fig. 1 where the end of the r process is associated to the drop in the heating rate). The peak becomes washed out at later times due to continuous production of material in this region by fission. However, neutron captures on the fission yields are responsible for a flow of matter from the second r-process peak to heavier nuclei. This flow operates in all used mass models except in FRDM due to the fact that material is halted at $N \sim 90$.

The situation at the third peak is different as the fission yields adopted here do not directly produce material in this region. The third peak abundance is noticeably more sensitive to nuclear masses that influence the neutron capture rates. It is not surprising that the abundances of this peak show a larger variation. However, for two of the mass models (FRDM, HFB21) the peak width is noticeably narrower than observed, the peak height is overestimated, the position shifted slightly to larger mass numbers and an abundance trough is predicted just above the peak. This is related to different behavior of these two models at the neutron number $N = 130$, just above the magic number $N = 126$. The FRDM and HFB21 mass models predict noticeably smaller neutron separation energies than the Duflo-Zuker or the WS3 models in this mass range. For example the nuclei ^{199}Yb , ^{198}Tm and ^{197}Er (all with $N = 129$) have neutron separation energies of $S_n = 0.52$ (0.85) MeV, 0.62 (0.73) MeV, and 0.26 (0.56) MeV, in the FRDM (HFB21) mass models [63], respectively, while they are 1.387 (1.463) MeV, 1.479 (1.528) MeV, and 0.908 (0.864) MeV for the same nuclei in the DZ31 (WS3) models. Thus these nuclei act as (additional) obstacles in r-process simulations using the FRDM and HFB21 mass models, even if the mass flow has overcome the $N = 126$ waiting points. As a result, the third peak in the abundance distribution is shifted for these two mass models to higher mass numbers as can be seen in Fig. 2 caused mainly by late-time neutron

captures. Due to the larger neutron separation energies, the $N = 130$ nuclei do not act as obstacles in simulations adopting the Duflo-Zuker or WS3 mass models. Relatedly the third peak develops at $A \sim 195$, associated with the $N = 126$ waiting points.

C. Evolution of the r-process abundances for fast ejecta

The characteristic of these trajectories is the very fast initial expansion which results in an r process operating at much lower densities than encountered for the ‘slow ejecta’. These low densities translate into a slow neutron depletion rate, with the important consequence, that a significant amount of neutrons remain at the end of the r process. (These neutrons will subsequently decay contributing to the late-time r-process heating as discussed below in Sec. III E.) Hence, we define the freeze-out for the fast ejecta at the moment when $\tau_{(n,\gamma)} = \tau_\beta$ rather than by $R_{n/s} = 1$, as done for the slow ejecta. Due to the initially large neutron-to-seed ratios, all trajectories with fast expansion undergo 1-3 fission cycles.

In Fig. 4 we show r-process abundances obtained for the fast ejecta at three different phases of the evolution and for the 4 different mass models. The top panel, for each mass model, shows the abundances before the “last” fission cycle, when the average mass number $\langle A \rangle$ reaches the final maximum. The middle panel exhibits the abundances for $\tau_{(n,\gamma)} = \tau_\beta$ and the lower panel shows the final r-process abundances at 1 Gyr. Due to the slower neutron capture rates, the r-process path for the fast ejecta runs noticeably closer to the region of stability; i.e. through less neutron-rich nuclei, than for the slow ejecta. This has several consequences. First, the position of third r-process peak, related to nuclei with magic neutron number $N = 126$, is shifted to larger mass numbers around $A \sim 200$. This can be seen by comparing the r-process abundances, obtained for the fast ejecta, at the times before the “last” fission cycle (top panels of Fig. 4), with those for the slow ejecta at freeze-out, exhibited in Fig. 2. Second, under the conditions of fast expansion, and slow neutron captures, the nuclei with magic neutron numbers $N = 82$ are a noticeable obstacle for the mass flow towards heavier nuclei. In particular, matter accumulates, already before the last fission cycle, at the double-magic nucleus ^{132}Sn which has a relatively long beta-decay half-life of ≈ 37 s, producing a pronounced peak. Third, neutron captures are too inefficient to replenish the region of $A \sim 280$ prior to the last fission cycle for most of the trajectories. As a consequence, the subsequent decay of these heavy nuclei by fission contributes only rather modestly to the r-process abundances around the second peak at $A \sim 130$, as can be seen in the lower panels of Fig. 4. However, the decay of matter beyond the third peak, after freeze-out, fills up the abundances around lead.

In contrast to the slow ejecta, the fast ejecta exhibit

a large spread in the final abundances observed between the different trajectories. This points to a very strong sensitivity to details of the astrophysical conditions and to the nuclear properties, if neutron captures are slow during the r process. In fact, the fast ejecta, encountered in our NS merger scenario, resemble a nucleosynthesis process somewhat between r process and s process, producing abundance peak structures shifted noticeable to larger mass numbers than observed in the solar r-process abundance distribution.

D. Robust r-process abundances

Fig. 5 shows the final abundances at times of 1 Gyr for all individual NS merger trajectories and for all the mass models. Additionally, the figure exhibits mass-averaged abundances for all trajectories (red curves), for the slow trajectories (green curves), and for the fast ejecta (blue curves), respectively. To better visualize the contribution of slow and fast ejecta to the total ejected mass we have multiplied the slow and fast trajectories and their averages by the fractional contribution of each ejecta, i.e. ~ 0.9 for the slow and ~ 0.1 for the fast ejecta

As already stressed above, the most striking feature of our calculations is the fact that the final abundances for mass numbers $A > 120$ are virtually identical, for a given mass model, for all the slow ejecta, while they vary noticeably for the fast ejecta. Furthermore, the total mass-averaged abundances show the same pattern as those for the slow ejecta, as these constitute the dominating part of the ejected mass. We hence conclude that dynamical ejecta of NS mergers show a robust r-process pattern, as already concluded in refs. [12–14], provided that Y_e in the ejecta remains low, see refs [16–18], as expected in dynamical ejecta of NS-black hole and very asymmetric NS-NS mergers. We will now discuss the origin of the robustness.

Thanks to the large neutron-to-seed ratio found in NS merger conditions the r process runs through 1–4 fission cycles, where trajectories with larger initial neutron-to-seed ratio obviously support more cycles. This so-called fission cycling has been suggested to be responsible of producing r-process abundances that are almost independent of the astrophysical conditions. Ref. [64] has suggested that fission cycling contributes to produce a steady β flow equilibrium in which the abundances for each isotopic chain are proportional to the beta-decay half-lives. Steady β flow equilibrium is in fact achieved in NS merger before the r-process freeze-out as the duration of the r process is longer than the individual beta-decay half-lives. Furthermore, it can be achieved both for hot and cold r-process conditions [59]. The upper panels of Fig. 2 show substantial differences in the r-process abundances for the different trajectories that nevertheless converge to a robust abundance pattern at the end of the calculations. This suggests that the mechanism responsible for producing a robust r-process pattern op-

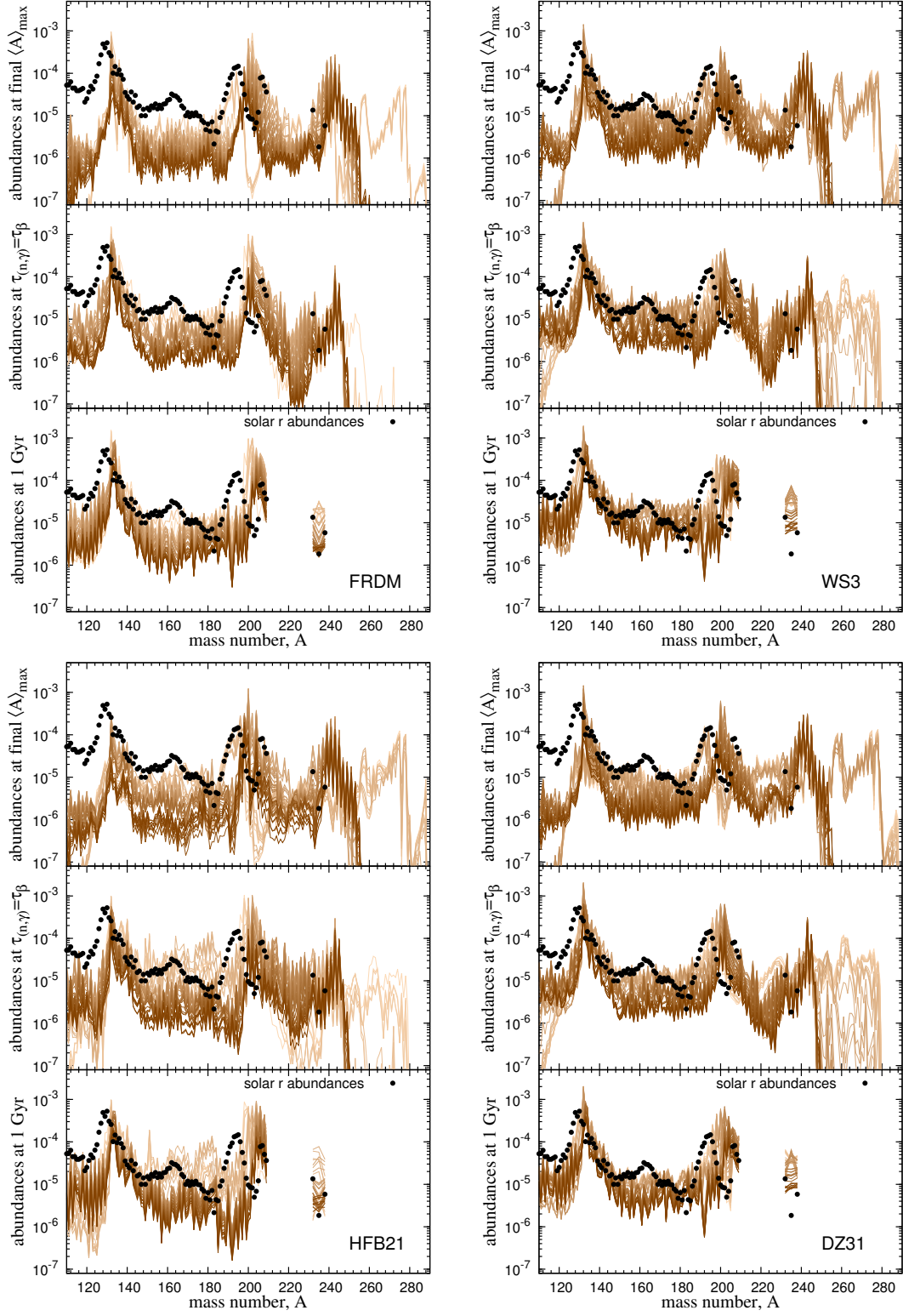


FIG. 4. (Color online) R-process abundances of fast ejecta for different mass models at different phases of the evolution. The upper panels show the abundances at times before the “last” fission cycle, when the average mass number $\langle A \rangle$ reaches the final maximum. The middle panel at the time where the average timescales for beta-decay and neutron captures become identical. The lower panel shows the abundances at 1 Gyr when most of the material has already decayed to the stability.

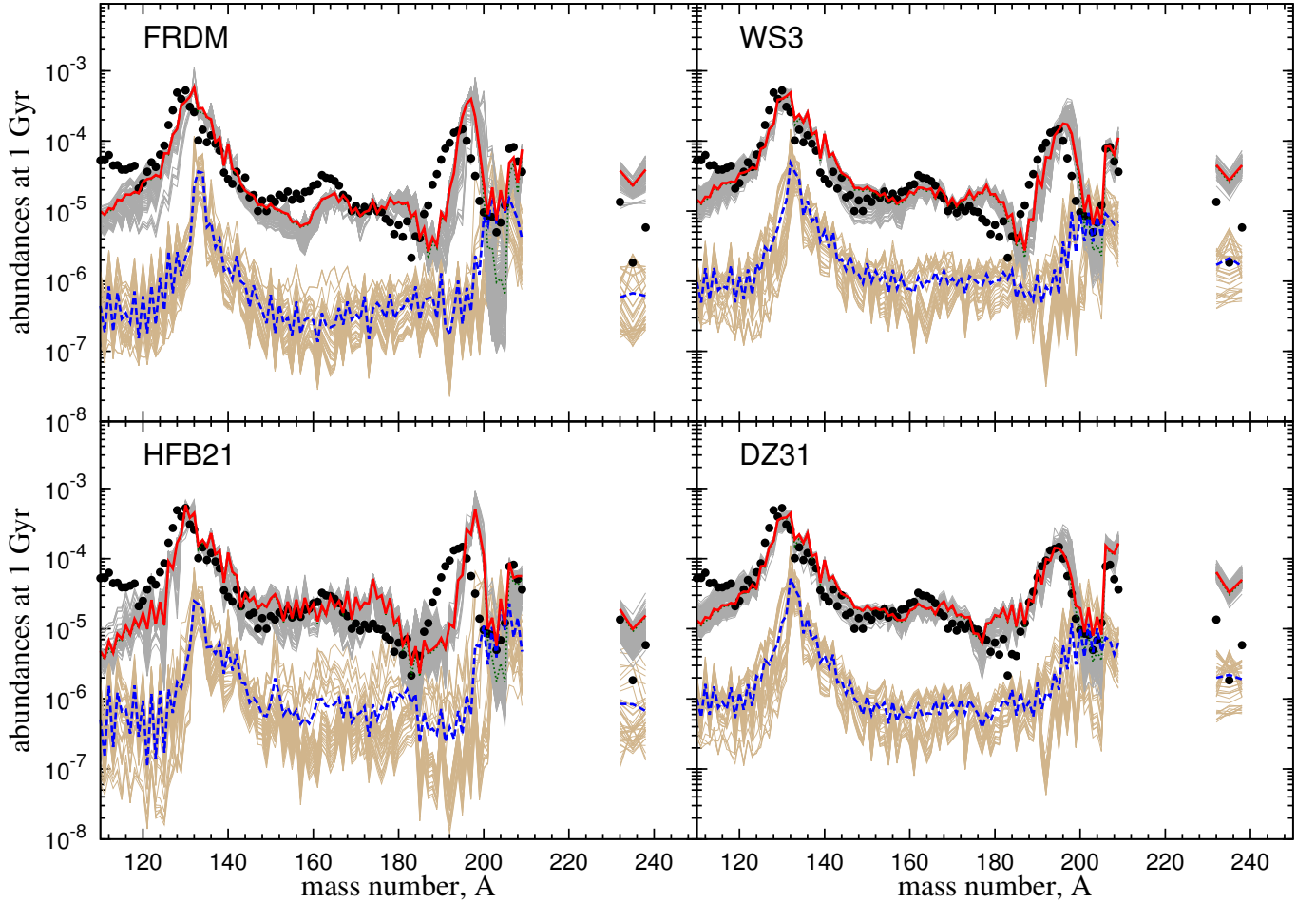


FIG. 5. (Color online) Final r-process abundances at a time of 1 Gyr for the different mass models and all trajectories used in the calculations. The grey (brown) curves correspond to the abundances of the trajectories of the slow (fast) ejecta shown previously in the bottom panels of Fig. 2 and 4 but without the color gradient. The mass-averaged abundances for all trajectories (red curves), the slow ejecta (green curves), and the fast ejecta (blue curves) are also shown. The abundances for the slow and fast trajectories and their averages have been scaled by the value of their fractional contribution to the total ejecta.

erates after r-process freeze-out and it is independent of the number of fission cycles.

We find that the main requirement to achieve a robust r-process pattern is that the amount of material accumulated at freeze-out in the fissioning region, $A \gtrsim 250$ is much larger than the one present in the region below the 3rd r-process peak. For the slow ejecta, this is guaranteed by the fact that the beta-decay half-lives grow with increasing mass number and by the presence of a neutron shell closure around $N = 184$. Both effects are responsible of producing a peak in the freeze-out r-process abundances around $A \sim 280$ (see upper panels Fig. 2). The material in this peak decays by fission contributing to the abundances around the 2nd r-process peak (see figure 3) and producing a final robust r-process pattern. For the fast ejecta, the lack of material accumulated in the $A > 250$ region, due to the much slower neutron capture rates at later stage of the r-process, results in reduced impact of fission yields on the final distributions and in a much larger spread of the final abundance distributions.

However, these trajectories contribute only mildly to the final mass-integrated abundances except for the region around $A = 200$.

The general features of this pattern is also independent of the mass models as it is mainly determined by fission yields. This is demonstrated in Fig. 6 where we compare the final mass-integrated abundances (at 1 Gyr) for four different mass models (FRDM, WS3, HFB21, DZ31). Although there are specific differences originating in the dependence of neutron captures on the underlying mass model, all the calculations reproduce the second and third r-process peaks reasonably well. We mention again that the peaks have different origins in our simulations: the peak around $A \sim 130$ arises from fission yields, while the peak at $A \sim 195$ reflects the $N = 126$ waiting points in the matter flow towards heavy nuclei. It is also satisfying to observe that the lead peak around $A \sim 208$ agrees reasonably well with the solar abundances. This peak is mainly produced by α decay of heavier nuclei. Finally also the abundances of the long-lived isotopes ^{232}Th

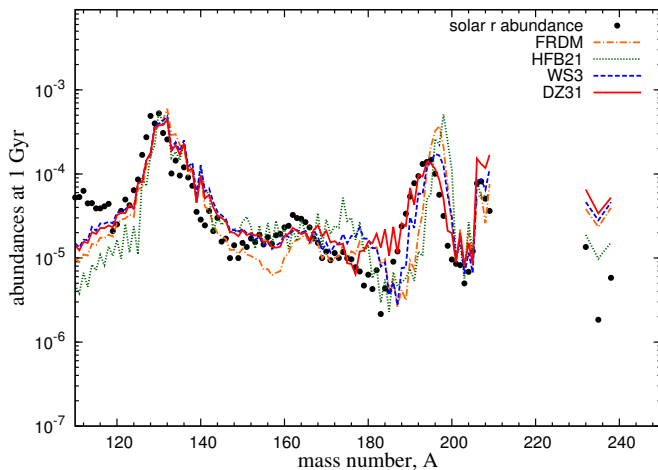


FIG. 6. (Color online) Final mass-integrated abundances for all trajectories at a time of 1 Gyr for all mass models considered in this work.

and ^{238}U , which are the final product of some matter with charge numbers $Z \approx 90 - 96$, is reproduced reasonably well.

In details, there are shortcomings of our various calculations when compared to the solar abundances. While the height and the width of the $A \sim 130$ peak are well described by all models, the peak position - mainly due to late-time neutron captures - is slightly shifted to larger mass numbers than observed. The similarity of all models in the description of this peak is related to the fact that we use the same fission yield distributions in all studies. Furthermore our description is noticeably improved compared with those of Refs. [12–14] due to the different fission barriers and yields used in the present work.

Goriely *et al.* [65] have recently presented a new fission fragment distribution model that predicts substantially different fission yields for r-process nuclei to those used in the present work. Given the important role that fission yields play in determining the r-process abundances, it is rather important to further study the sensitivity of the r-process abundances to the fission yields, including the recently developed GEF model [66–68], and explore experimental possibilities to constrain them. This goes beyond the goals of the present work.

E. Implications for kilonova observations

One of the most interesting consequences of r-process nucleosynthesis in neutron star mergers is that the large amount of material ejected can produce an electromagnetic transient powered by the radioactive decay of r-process nuclei [12, 14, 56, 69–71]. This transient is commonly denoted as kilonova and may have been recently observed associated with the short γ -ray burst GRB130603B [72, 73].

Modeling kilonova light curves requires the knowledge

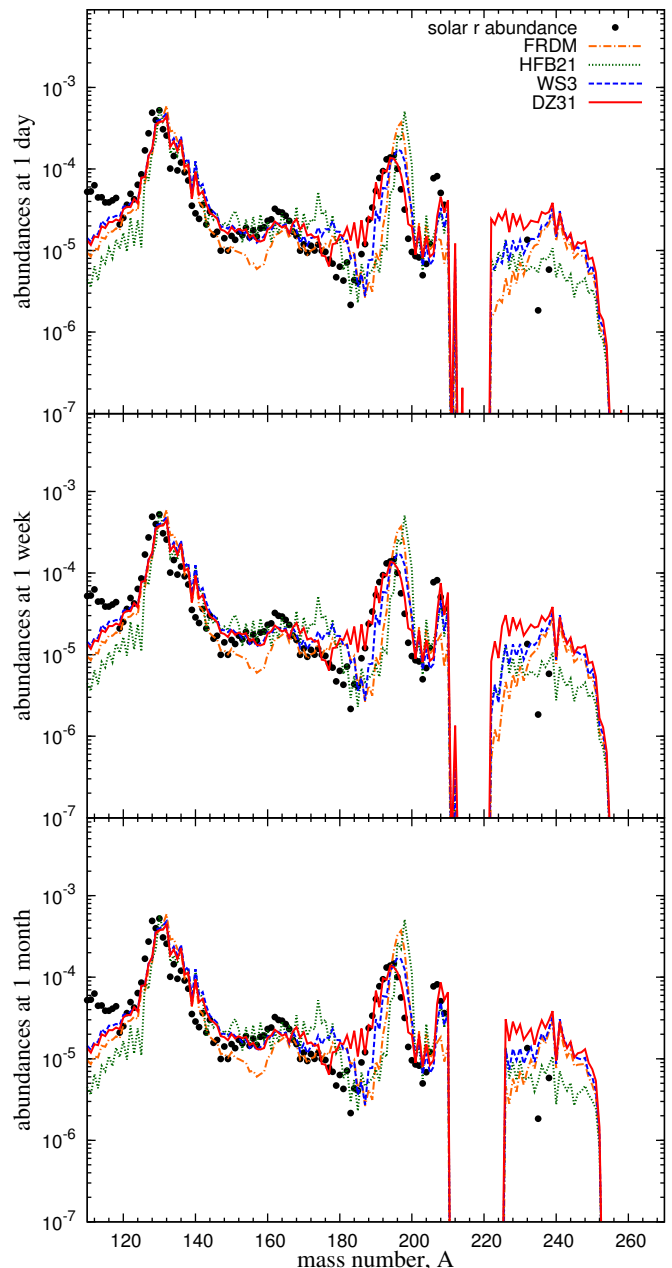


FIG. 7. (Color online) Mass- r-process abundances on timescales of a day (upper panel), a week (middle panel) and a month (lower panel) after the r-process event for the different mass models considered in the present study.

of the r-process heating rates at timescales between hours and weeks and identify those nuclei that predominantly contribute to the heating rate. This aspect will be explored in further work. In addition, it is also important to know the optical opacities for r-process material as they determine the timescale for photons to escape from the inner opaque region of the ejecta. It has been suggested that a major source of opacity is due to the presence of lanthanides ($Z = 57-71$, $A \approx 139-176$) [74–76] in the r-process ejecta. Due to their large photon opacities

the lanthanides delay the light curve luminosity peak to timescales of a week. The peak frequency is also shifted to the red. An additional source of opacity could be due to the presence of actinides in the r-process ejecta. The r process in NS mergers ejecta is known to produce the actinides U and Th (see for example Fig. 6). However, at timescales of weeks relevant to kilonova observations the abundance of actinides ($Z = 89\text{--}103$, $A \approx 225\text{--}260$) can be much larger since many of the nuclei involved have long decay half-lives. This is confirmed in Fig. 7 that shows the mass-integrated r-process abundances at timescales of one day, one week and one month. As can be seen from Fig. 2, we find a rather small dependence of the actinide abundances on the astrophysical conditions. There is a much larger dependence on the nuclear physics input (see Figs. 2 and 7). This aspect requires further exploration. However, our results already show a strong correlation between the behavior of neutron separation energies around $N \sim 130$ and the amount of actinides produced. Mass models that predict low neutron separation energies tend to accumulate more material in the third r-process peak and predict lower abundances for actinides.

On top of the light curves due to the r-process heating, neutrons that survived after the r process in the fast ejecta will decay and may provide another electromagnetic probe for the neutron star mergers that peaks hours after merger [37]. One important quantity in determining the luminosity and the frequency peak of this neutron-decay powered light curves is the amount of free neutrons after the r process. We find in our calculations that this amount is rather sensitive to the nuclear mass model adopted. For the four different mass models we have explored, the total mass of free neutrons at ~ 20 second post-merger is a sizable fraction of the total mass of the fast ejecta and amounts to 5.39×10^{-5} , 4.42×10^{-5} , 2.86×10^{-5} , and $2.68 \times 10^{-5} M_\odot$ for the FRDM, HFB21, WS3, and DZ31 mass model, respectively. This sensitivity of the mass model is due to the same reason discussed above that the low neutron separation energies predicted by FRDM and HFB21 give rise to the smaller neutron capture rates around the third peak such that there are free neutrons left at the end of the r process, when compared to the WS3 and DZ31 mass model. Moreover, we note that the opacity due to the r-process nuclei for the fast ejecta may be somewhat different from the slow ejecta which in turn may also affect the detailed modeling of the kilonova light curves.

IV. CONCLUSIONS

In summary, we have performed r-process simulations for matter ejected in neutron star merger calculations. Due to the extreme neutron-to-seed ratios achieved, which favor mass transport to the region of fissioning nuclei, fission rates and yields are crucial ingredients in such calculations. Adopting these quantities from the

ABLA code which has been adjusted to reproduce fission and fragmentation data and treats the release of neutrons during the fission process explicitly, we have been able to reproduce the main features of the r-process abundances (the second and third peaks, the rare-earth peak and the lead peak) reasonably well. Importantly, we found that these features do not depend sensitively on the astrophysical conditions for the majority of the ejecta (but see Ref. [16–18] for a possible increase of the initial electron fraction which may have an impact on the abundance patterns). We have also shown that these features do not depend in general on the nuclear mass model used. We noticed, however, modest differences in the position of the third peak and in abundance distribution just above this peak around $A \sim 205$. Here the FRDM and HFB21 mass models predict noticeably smaller neutron separation energies for r-process nuclei with $N = 130$ than the other mass models used in our studies. These small separation energies make the $N = 130$ nuclei obstacles in the r-process path resulting in the peak shift and a pronounced abundance trough at $A \sim 205$, if compared to the solar r-process abundances. Experimental work is needed to resolve these different mass predictions for the $N = 130$ nuclei.

Our simulations support the hypothesis that the r process in dynamical ejecta from neutron star mergers yield rather robust abundance distribution (provided Y_e of the ejecta is sufficiently low) in good agreement with the observed solar distribution for nuclei with $A \gtrsim 120$. We have shown that a requirement to achieve such a robust pattern is that at freeze-out the amount of material accumulated in the fissioning region ($A \gtrsim 250$) is much larger than the material located in the second r-process peak and above ($A \approx 120\text{--}180$). To achieve these astrophysical conditions, a sufficiently large neutron-to-seed ratio is required, which, together with the fact that beta-decay half-lives along the r-process path grow with increasing mass number, guarantees the pile up of material in the fissioning region. The decay of this material by fission produces a robust r-process pattern in the region $A \approx 120\text{--}180$ that, however, depends on the used fission yields (see ref. [77]). This pattern is slightly modified by neutron captures during the decay back to stability, which also introduces a small dependence of the abundance patterns on the astrophysical conditions. In this scenario, larger neutron-to-seed ratios only increase the amount of fission cycles without modifying the final r-process abundance distribution. These, however, might be sensitive to the detailed shell structure in the mass region of fissioning nuclei and, in particular, to the strength of the $N = 184$ shell closure.

Finally, in our simulation, $\sim 10\%$ of the ejecta expand so fast that the resulting r-process operates at much lower neutron number densities. Consequently, the nucleosynthesis path is closer to stability with significantly less amount of fissioning nuclei present at the time of freeze-out. Hence, the fission yields do not contribute much to the final abundances at the second r-process

peak and the second and third r-process peaks shift to larger mass numbers. Furthermore, there exists a large variation in the final abundances between different trajectories, in clear contrast to the slow ejecta. In addition, a significant amount of neutrons is left at the end of the r process. This amount, however, depends sensitively on the nuclear mass model input.

The observation of electromagnetic signals of the r process is an intriguing possibility. In this context our simulations imply that for most of the mass models used the amount of actinides present at timescales of several weeks is similar or larger than that of lanthanides. Consequently, actinides may dominate the photon opacities for kilonova light curves. The differences in abundance pattern and, also, the amount of free neutrons present at the end of the r process for fast ejecta might be relevant for detailed modelling of these light curves.

Current constraints on the NS merger rate are compatible with NS-NS and/or NS-black hole mergers being the dominant source of r-process elements in our galaxy [78]. It is not excluded that the NS merger scenario is responsible also for the solar-like r-process patterns observed in old, metal-poor stars. This requires, however, that the frequency of neutron star mergers is sufficiently large during the early evolution of the Milky Way, which is a topic currently being explored in the context of dynamical galactic chemical evolution models [79, 80].

Further extensions of the present work, need to address the impact of variations of fission rates and beta-decay rates. In this study, we have limited the variation of nuclear masses to nuclei with $Z < 83$ as for heavier nuclei fission rates have not been computed consistently with the mass models used. Given the fundamental role played by fission in dynamical ejecta of neutron star mergers, it is very important to consistently determine both nuclear masses and fission relevant quantities. These include both fission barriers and collective inertial masses. Recent global calculations [81–83] have mainly focussed on the description of fission barriers neglecting the important role of collective masses that are normally described using a simple phenomenological prescription [84] in r-

process applications. Furthermore, it is important to address the impact of dynamical versus static descriptions of fission observables [85, 86].

Beta-decay half-lives have not been consistently computed with the mass models explored in this work. Ideally, one should use the same model applied for the calculation of nuclear masses to determine the Gamow-Teller and first-forbidden strengths that determine the beta-decay half-lives of r-process nuclei. Consistency between the calculations of masses and beta-decay half-lives can in principle be achieved in mean-field approaches by performing quasiparticle random phase approximation calculations where the residual interaction is derived from the same density functional used for the calculation of nuclear masses [58, 87]. However, this approach does not uniquely determines the computed beta-decay half-lives as they are quite sensitive to the choice of proton-neutron $T = 0$ pairing [87, 88] while this interaction channel barely affects the masses of neutron-rich r-process nuclei.

ACKNOWLEDGMENTS

Helpful conversations with Marius Eichler and Friedel Thielemann about the role of neutrons produced by fission in r-process nucleosynthesis are acknowledged. This work was supported by the Deutsche Forschungsgemeinschaft through contract SFB 634, the Helmholtz International Center for FAIR within the framework of the LOEWE program launched by the state of Hesse, the Helmholtz Association through the Nuclear Astrophysics Virtual Institute (VH-VI-417) and the ExtreMe Matter Institute EMMI in the framework of the Helmholtz Alliance HA216/EMMI. A.B. is a Marie Curie Intra-European Fellow within the 7th European Community Framework Programme (IEF 331873). This work was supported by the Deutsche Forschungsgemeinschaft through Sonderforschungsbereich Transregio 7 “Gravitational Wave Astronomy”, and the Cluster of Excellence EXC 153 “Origin and Structure of the Universe”.

-
- [1] E. M. Burbidge, G. R. Burbidge, W. A. Fowler, and F. Hoyle, *Rev. Mod. Phys.* **29**, 547 (1957).
 - [2] A. G. W. Cameron, *Stellar Evolution, Nuclear Astrophysics, and Nucleogenesis*, Report CRL-41 (Chalk River, 1957).
 - [3] J. J. Cowan, F.-K. Thielemann, and J. W. Truran, *Phys. Repts.* **208**, 267 (1991).
 - [4] M. Arnould, S. Goriely, and K. Takahashi, *Phys. Repts.* **450**, 97 (2007).
 - [5] S. E. Woosley, J. R. Wilson, G. J. Mathews, R. D. Hoffman, and B. S. Meyer, *Astrophys. J.* **433**, 229 (1994).
 - [6] H.-T. Janka, *Ann. Rev. of Nucl. Part. Sci.* **62**, 407 (2012).
 - [7] G. Martínez-Pinedo, T. Fischer, A. Lohs, and L. Huther, *Phys. Rev. Lett.* **109**, 251104 (2012).
 - [8] L. F. Roberts, S. Reddy, and G. Shen, *Phys. Rev. C* **86**, 065803 (2012).
 - [9] G. Martínez-Pinedo, T. Fischer, and L. Huther, *J. Phys. G: Nucl. Part. Phys.* **41**, 044008 (2014).
 - [10] J. M. Lattimer and D. N. Schramm, *Astrophys. J.* **192**, L145 (1974).
 - [11] C. Freiburghaus, S. Rosswog, and F.-K. Thielemann, *Astrophys. J.* **525**, L121 (1999).
 - [12] S. Goriely, A. Bauswein, and H.-T. Janka, *Astrophys. J.* **738**, L32 (2011).
 - [13] O. Korobkin, S. Rosswog, A. Arcones, and C. Winteler, *Mon. Not. Roy. Astron. Soc.* **426**, 1940 (2012).
 - [14] A. Bauswein, S. Goriely, and H.-T. Janka, *Astrophys. J.* **773**, 78 (2013).
 - [15] C. Sneden, J. J. Cowan, and R. Gallino, *Annu. Rev. Astron. Astrophys.* **46**, 241 (2008).

- [16] S. Wanajo, Y. Sekiguchi, N. Nishimura, K. Kiuchi, K. Kyutoku, and M. Shibata, *Astrophys. J.* **789**, L39 (2014).
- [17] Y. Sekiguchi, K. Kiuchi, K. Kyutoku, and M. Shibata, *Phys. Rev. D* **91**, 064059 (2015).
- [18] S. Goriely, A. Bauswein, O. Just, E. Pllumbi, and H.-T. Janka, *Mon. Not. Roy. Astron. Soc.* **452**, 3894 (2015).
- [19] R. Fernández and B. D. Metzger, *Mon. Not. Roy. Astron. Soc.* **435**, 502 (2013).
- [20] O. Just, A. Bauswein, R. A. Pulpillo, S. Goriely, and H.-T. Janka, *Mon. Not. Roy. Astron. Soc.* **448**, 541 (2015).
- [21] B. D. Metzger and R. Fernández, *Mon. Not. Roy. Astron. Soc.* **441**, 3444 (2014).
- [22] A. Perego, S. Rosswog, R. M. Cabezón, O. Korobkin, R. Käppeli, A. Arcones, and M. Liebendörfer, *Mon. Not. Roy. Astron. Soc.* **443**, 3134 (2014).
- [23] M. Eichler, A. Arcones, A. Kelic, O. Korobkin, K. Langanke, T. Marketin, G. Martínez-Pinedo, I. Panov, T. Rauscher, S. Rosswog, C. Winteler, N. T. Zinner, and F.-K. Thielemann, *Astrophys. J.* **808**, 30 (2015).
- [24] J.-J. Gaimard and K.-H. Schmidt, *Nucl. Phys. A* **531**, 709 (1991).
- [25] A. Kelic, M. Valentina Ricciardi, and K.-H. Schmidt, ArXiv e-prints (2009), [arXiv:0906.4193 \[nucl-th\]](#).
- [26] O. L. Caballero, A. Arcones, I. N. Borzov, K. Langanke, and G. Martínez-Pinedo, ArXiv e-prints (2014), [arXiv:1405.0210 \[nucl-th\]](#).
- [27] I. Borzov, *Nucl. Phys. A* **777**, 645 (2006).
- [28] T. Kurtukian-Nieto, J. Benlliure, K.-H. Schmidt, L. Audouin, F. Becker, B. Blank, I. Borzov, E. Casarejos, F. Farget, M. Fernández-Ordóñez, J. Giovinazzo, D. Henzlova, B. Jurado, K. Langanke, G. Martínez-Pinedo, J. Pereira, and O. Yordanov, *Eur. Phys. J. A* **50**, 135 (2014).
- [29] Q. Zhi, E. Caurier, J. J. Cuenca-García, K. Langanke, G. Martínez-Pinedo, and K. Sieja, *Phys. Rev. C* **87**, 025803 (2013).
- [30] T. Suzuki, T. Yoshida, T. Kajino, and T. Otsuka, *Phys. Rev. C* **85**, 015802 (2012).
- [31] P. Möller, J. R. Nix, W. D. Myers, and W. J. Swiatecki, *At. Data Nucl. Data Tables* **59**, 185 (1995).
- [32] J. M. Pearson, R. C. Nayak, and S. Goriely, *Phys. Lett. B* **387**, 455 (1996).
- [33] M. Liu, N. Wang, Y. Deng, and X. Wu, *Phys. Rev. C* **84**, 014333 (2011).
- [34] J. Duflo and A. P. Zuker, *Phys. Rev. C* **52**, R23 (1995).
- [35] S. Goriely, N. Chamel, and J. M. Pearson, *Phys. Rev. Lett.* **102**, 152503 (2009).
- [36] S. Goriely, N. Chamel, and J. M. Pearson, *Phys. Rev. C* **82**, 035804 (2010).
- [37] B. D. Metzger, A. Bauswein, S. Goriely, and D. Kasen, *Mon. Not. Roy. Astron. Soc.* **446**, 1115 (2015).
- [38] R. Oechslin, S. Rosswog, and F.-K. Thielemann, *Phys. Rev. D* **65**, 103005 (2002).
- [39] R. Oechslin, H.-T. Janka, and A. Marek, *Astron. & Astrophys.* **467**, 395 (2007).
- [40] A. Bauswein, H.-T. Janka, and R. Oechslin, *Phys. Rev. D* **82**, 084043 (2010).
- [41] J. Isenberg and J. Nester, in *One hundred years after the birth of Albert Einstein*, General Relativity and Gravitation, Vol. 1, edited by A. Held (Plenum Press, New York, 1980) p. 23.
- [42] J. R. Wilson, G. J. Mathews, and P. Marronetti, *Phys. Rev. D* **54**, 1317 (1996).
- [43] M. Ruffert, H.-T. Janka, K. Takahashi, and G. Schaefer, *Astron. & Astrophys.* **319**, 122 (1997).
- [44] Y. Sugahara and H. Toki, *Nucl. Phys. A* **579**, 557 (1994).
- [45] M. Hempel, T. Fischer, J. Schaffner-Bielich, and M. Liebendörfer, *Astrophys. J.* **748**, 70 (2012).
- [46] A. W. Steiner, M. Hempel, and T. Fischer, *Astrophys. J.* **774**, 17 (2013).
- [47] J. M. Lattimer, *Annu. Rev. Nucl. Part. Sci.* **62**, 485 (2012).
- [48] H. P. Loens, Ph.D. thesis, TU Darmstadt (2010).
- [49] P. Möller, B. Pfeiffer, and K.-L. Kratz, *Phys. Rev. C* **67**, 055802 (2003).
- [50] T. Dong and Z. Ren, *Eur. Phys. J. A* **26**, 69 (2005).
- [51] I. V. Panov, I. Y. Korneev, T. Rauscher, G. Martínez-Pinedo, A. Kelić-Heil, N. T. Zinner, and F. Thielemann, *Astron. & Astrophys.* **513**, A61 (2010).
- [52] W. D. Myers and W. J. Świątecki, *Phys. Rev. C* **60**, 014606 (1999).
- [53] I. Petermann, K. Langanke, G. Martínez-Pinedo, I. V. Panov, P.-G. Reinhard, and F.-K. Thielemann, *Eur. Phys. J. A* **48**, 122 (2012).
- [54] N. T. Zinner, Ph.D. thesis, University of Aarhus, Denmark (2007).
- [55] B. D. Metzger, A. Arcones, E. Quataert, and G. Martínez-Pinedo, *Mon. Not. Roy. Ast. Soc.* **402**, 2771 (2010).
- [56] B. D. Metzger, G. Martínez-Pinedo, S. Darbha, E. Quataert, A. Arcones, D. Kasen, R. Thomas, P. Nugent, I. V. Panov, and N. T. Zinner, *Mon. Not. Roy. Ast. Soc.* **406**, 2650 (2010).
- [57] F. X. Timmes and D. Arnett, *Astrophys. J. Suppl.* **125**, 277 (1999).
- [58] T. Marketin, L. Huther, and G. Martínez-Pinedo, ArXiv e-prints (2015), [arXiv:1507.07442 \[nucl-th\]](#).
- [59] A. Arcones and G. Martínez-Pinedo, *Phys. Rev. C* **83**, 045809 (2011).
- [60] B. S. Meyer, G. J. Mathews, W. M. Howard, S. E. Woosley, and R. D. Hoffman, *Astrophys. J.* **399**, 656 (1992).
- [61] J. Hakala, J. Dobaczewski, D. Gorelov, T. Eronen, A. Jokinen, A. Kankainen, V. S. Kolhinen, M. Kortelainen, I. D. Moore, H. Penttilä, S. Rinta-Antila, J. Rissanen, A. Saastamoinen, V. Sonnenschein, and J. Äystö, *Phys. Rev. Lett.* **109**, 032501 (2012).
- [62] J. Van Schelt, D. Lascar, G. Savard, J. A. Clark, S. Caldwell, A. Chaudhuri, J. Fallis, J. P. Greene, A. F. Levand, G. Li, K. S. Sharma, M. G. Sternberg, T. Sun, and B. J. Zabransky, *Phys. Rev. C* **85**, 045805 (2012).
- [63] We note that the low neutron separation energies remain in the latest version of the HFB type mass model, HFB27 [89].
- [64] J. Beun, G. C. McLaughlin, R. Surman, and W. R. Hix, *Phys. Rev. C* **77**, 035804 (2008).
- [65] S. Goriely, J.-L. Sida, J.-F. Lemaître, S. Panebianco, N. Dubray, S. Hilaire, A. Bauswein, and H.-T. Janka, *Phys. Rev. Lett.* **111**, 242502 (2013).
- [66] K.-H. Schmidt and B. Jurado, *Phys. Rev. Lett.* **104**, 212501 (2010).
- [67] K.-H. Schmidt and B. Jurado, *Phys. Rev. C* **83**, 061601 (2011); *Phys. Rev. C* **84**, 059906 (2011).
- [68] K.-H. Schmidt, B. Jurado, and C. Amouroux, *General Description of Fission Observables: GEF model*, JEFF Report 24 (OECD Nuclear Energy Agency, 2014).

- [69] L. Li and B. Paczyński, *Astrophys. J.* **507**, L59 (1998).
- [70] S. R. Kulkarni, ArXiv Astrophysics e-prints (2005), [astro-ph/0510256](#).
- [71] L. F. Roberts, D. Kasen, W. H. Lee, and E. Ramirez-Ruiz, *Astrophys. J.* **736**, L21 (2011).
- [72] N. R. Tanvir, A. J. Levan, A. S. Fruchter, J. Hjorth, R. A. Hounsell, K. Wiersema, and R. L. Tunnicliffe, *Nature* **500**, 547 (2013).
- [73] E. Berger, W. Fong, and R. Chornock, *Astrophys. J.* **774**, L23 (2013).
- [74] D. Kasen, N. R. Badnell, and J. Barnes, *Astrophys. J.* **774**, 25 (2013).
- [75] J. Barnes and D. Kasen, *Astrophys. J.* **775**, 18 (2013).
- [76] M. Tanaka and K. Hotokezaka, *Astrophys. J.* **775**, 113 (2013).
- [77] S. Goriely and G. Martínez-Pinedo, *Nucl. Phys. A* (2015), [10.1016/j.nuclphysa.2015.07.020](#).
- [78] A. Bauswein, R. Ardevol Pulpillo, H.-T. Janka, and S. Goriely, *Astrophys. J.* **795**, L9 (2014).
- [79] F. van de Voort, E. Quataert, P. F. Hopkins, D. Kereš, and C.-A. Faucher-Giguère, *Mon. Not. Roy. Astron. Soc.* **447**, 140 (2015).
- [80] S. Shen, R. J. Cooke, E. Ramirez-Ruiz, P. Madau, L. Mayer, and J. Guedes, *Astrophys. J.* **807**, 115 (2015).
- [81] S. Goriely, S. Hilaire, A. J. Koning, M. Sin, and R. Capote, *Phys. Rev. C* **79**, 024612 (2009).
- [82] P. Möller, A. J. Sierk, T. Ichikawa, A. Iwamoto, R. Bengtsson, H. Uhrenholt, and S. Åberg, *Phys. Rev. C* **79**, 064304 (2009).
- [83] J. Erler, K. Langanke, H. Loens, G. Martínez-Pinedo, and P.-G. Reinhard, *Phys. Rev. C* **85**, 025802 (2012).
- [84] S. Goriely, *Eur. Phys. J. A* **51**, 22 (2015).
- [85] J. Sadhukhan, K. Mazurek, A. Baran, J. Dobaczewski, W. Nazarewicz, and J. A. Sheikh, *Phys. Rev. C* **88**, 064314 (2013).
- [86] S. A. Giuliani, L. M. Robledo, and R. Rodríguez-Guzmán, *Phys. Rev. C* **90**, 054311 (2014).
- [87] J. Engel, M. Bender, J. Dobaczewski, W. Nazarewicz, and R. Surman, *Phys. Rev. C* **60**, 014302 (1999).
- [88] Z. M. Niu, Y. F. Niu, H. Z. Liang, W. H. Long, T. Nikšić, D. Vretenar, and J. Meng, *Phys. Lett. B* **723**, 172 (2013).
- [89] S. Goriely, N. Chamel, and J. M. Pearson, *Phys. Rev. C* **88**, 061302 (2013).